

RESEARCH

Open Access



Keratin 15 protects against cigarette smoke-induced epithelial mesenchymal transformation by MMP-9

Wensi Zhu^{1,4,5†}, Linxiao Han^{1,4,5†}, Yuanyuan Wu^{1,4,5†}, Lin Tong^{1,4,5†}, Ludan He^{3,4,5†}, Qin Wang^{1,4,5}, Yu Yan^{1,4,5}, Ting Pan^{1,4,5}, Jie Shen^{7,8,9}, Yuanlin Song^{3,5}, Yao Shen^{2*}, Qiaoliang Zhu^{6*} and Jian Zhou^{1,4,5,7,8,9*}

Abstract

Background Chronic obstructive pulmonary disease (COPD), a chronic inflammatory lung disease, is a leading cause of morbidity and mortality worldwide. Prolonged cigarette smoking (CS) that causes irreversible airway remodeling and significantly reduces lung function is a major risk factor for COPD. Keratin15⁺ (Krt15⁺) cells with the potential of self-renewal and differentiation properties have been implicated in the maintenance, proliferation, and differentiation of airway basal cells; however, the role of Krt15 in COPD is not clear.

Methods Krt15 knockout (Krt15^{-/-}) and wild-type (WT) mice of C57BL/6 background were exposed to CS for six months to establish COPD models. *Krt15-CrePGR;Rosa26-LSL-tdTomato* mice were used to trace the fate of the Krt15⁺ cells. Hematoxylin and eosin (H&E) and Masson stainings were performed to assess histopathology and fibrosis, respectively. Furthermore, lentivirus-delivered short hairpin RNA (shRNA) was used to knock down KRT15 in human bronchial epithelial (HBE) cells stimulated with cigarette smoke extract (CSE). The protein expression was assessed using western blot, immunohistochemistry, and enzyme-linked immunosorbent assay.

Results Krt15^{-/-} CS mice developed severe inflammatory cell infiltration, airway remodeling, and emphysema. Moreover, Krt15 knockout aggravated CS-induced secretion of matrix metalloproteinase-9 (MMP-9) and epithelial–mesenchymal transformation (EMT), which was reversed by SB-3CT, an MMP-9 inhibitor. Consistent with this finding, KRT15 knockdown promoted MMP-9 expression and EMT progression in vitro. Furthermore, Krt15⁺ cells gradually increased in the bronchial epithelial cells and were transformed into alveolar type II (AT2) cells.

Conclusion Krt15 regulates the EMT process by promoting MMP-9 expression and protects the lung tissue from CS-induced injury, inflammatory infiltration, and apoptosis. Furthermore, Krt15⁺ cells transformed into AT2 cells to protect alveoli. These results suggest Krt15 as a potential therapeutic target for COPD.

Keywords Airway remodeling, Chronic obstructive pulmonary disease, Inflammatory infiltration, Matrix metalloproteinase-9

[†]Wensi Zhu, Linxiao Han, Yuanyuan Wu, Lin Tong and Ludan He contributed equally to this work.

*Correspondence:

Yao Shen

13611692261@163.com

Qiaoliang Zhu

zhuqiaoliang111@126.com

Jian Zhou

zhoujian@fudan.edu.cn

Full list of author information is available at the end of the article



Introduction

Chronic obstructive pulmonary disease (COPD) is the third most common cause of death and is associated with high morbidity and mortality rates worldwide. In 2019, approximately 212.3 million epidemic cases of COPD have been reported globally [1]. COPD is characterized by persistent airflow limitation and irreversible airway remodeling and can be diagnosed by the presence of a post-bronchodilator forced expiratory volume in one second/forced vital capacity value of <0.7 ($FEV_1/FVC < 0.7$) [2]. Smoking is the most common risk factor for COPD. Although the pathogenesis of COPD is still unclear, numerous studies have shown that long-term cigarette smoking (CS) exposure causes airway basal cell reprogramming and alveolar damage and triggers airway remodeling and emphysema (destruction and enlargement of alveoli) [3–5]. COPD increases the small airway resistance leading to obstruction of the air passage, which consequently causes obstructive bronchitis. Despite the high mortality rates [6] (3.3 million people die due to COPD) and the serious effects of COPD on human health and quality of life, a few drugs can repair damaged airways and promote lung regeneration.

The main pathological features of COPD include irregular inflammatory patterns and airway and parenchymal remodeling, which eventually leads to irreversible fibrosis and occlusion of small airways [7]. Epithelial–mesenchymal transition (EMT) plays an important role in small airway remodeling and subepithelial fibrosis. EMT is divided into three main types: type 1, which mainly occurs during embryonic development; type 3, which is significantly associated with epithelial malignancies; and type 2, which mainly occurs during organ fibrosis [8]. Several studies have shown that type 2 EMT is active in the small airways of patients with COPD [9–11]. During EMT, epithelial cells lose polarity and adhesion and then transit to a mesenchymal phenotype, which is characterized by a significant reduction in the expression of the epithelial cell marker E-cadherin and a significant increase in the expression of mesenchymal cell markers such as vimentin and S100A4 [12, 13]. At present, the drugs used for the treatment of COPD, such as bronchodilators, corticosteroids, and β_2 -agonists, can only alleviate the symptoms [14], but cannot reverse or delay airway remodeling. Therefore, further identification of the molecular mechanisms mediating EMT and the exploration of more effective and safe strategies that might attenuate EMT and hinder small airway remodeling is of immense practical benefit for preventing and treating COPD.

Keratin 5 (Krt5) dimerizes with Krt14 and forms the intermediate filaments underlying the basal epithelial cell cytoskeleton. Krt15, a type I keratin [15], has been

shown to compensate for the lack of Krt14 and dimerizes with Krt5 to form keratin intermediate filaments [16]. Krt15 was first detected in the hair follicle bulges and its expression was shown to be correlated with epidermal cells [17]. Several studies have demonstrated that the expression of Krt15 is increased during hair follicle growth, differentiation, growth of the lacrimal gland, and epidermal injury repair [18–21]. In addition, Krt15⁺ precursor cells have been implicated in basal cell carcinoma [22, 23]. Krt15 has also been shown to be upregulated in a subset of urothelial cell carcinomas and mark the basal epithelia in ureters [24]. Krt15 also marks a population of long-lived progenitor cells in the mouse esophageal epithelium, which are capable of self-renewal, proliferation, and differentiation [25]. Krt15 has also been detected in the crypt cells of the small intestine, marking long-lived pluripotent crypt cells with self-renewal ability and radiation resistance, which play an important role in tissue regeneration after injury [20]. Together, these studies indicated that Krt15 is strongly associated with the repair and regeneration of tissue cells after injury. Recently, it has also been shown that when Krt15 in airway basal cells is switched to Krt14, the clonogenicity of airway basal cells decreases [26]. However, the role of Krt15 in COPD remains unclear.

We hypothesized that Krt15 mediates airway remodeling by regulating EMT. To validate this hypothesis, we first traced the dynamic changes in Krt15⁺ cells exposed to CS in reporter mice using genetic lineage tracing. The relationship between Krt15 and EMT was investigated by exposing Krt15^{-/-} mice to CS for 6 months and human bronchial epithelial (HBE) stimulated with cigarette smoke extract (CSE).

Material and methods

Bioinformatics and computational analysis

KRT15 mRNA expression data from RNA-seq datasets (GSE5058 and GSE8545) were obtained from the GEO database (<https://www.ncbi.nlm.nih.gov/geo/>). Only nonsmokers and patients with COPD were included in both datasets to analyze the expression levels of KRT15. The “GEOquery” [2.54.1] and “limma” [3.42.2] packages in R version 3.6.3 were used for the statistical analysis.

Establishment of COPD models and animal grouping

C57BL/6 mice (8–10 weeks old) were purchased from Shanghai Model Organisms Center, Inc. (Shanghai, China). Krt15 knockout mice (Krt15^{-/-}) were generated using the CRISPR-Cas9 gene editing technology at Shanghai Model Organisms Center, Inc. The mice were randomly divided into four groups based on their CS regimes: (I) wild-type (WT), (II) Krt15^{-/-}, (III) WT CS, and (IV) Krt15^{-/-} CS with 6 mice in each group. WT CS

and $Krt15^{-/-}$ CS mice were exposed to CS for 6 months (4 h/day, 20 cigarettes/day, Daqianmen, Shanghai, China) in an acrylic box (75×75×45 cm) to establish COPD models [25, 27, 28].

Krt15-CrePGR;Rosa26-LSL-tdTomato mice were used to trace the fate of $Krt15^+$ cells. These mice were intraperitoneally injected with 25 mg/kg/day RU486 (M8046, Sigma-Aldrich, Saint Louis, MO, USA) that were dissolved in corn oil for 5 days for Cre recombination. The mice were divided into six groups based on their smoking exposure: (I) $R26^{mT}$ -14d, (II) $R26^{mT}$ CS-14d, (III) $R26^{mT}$ -30d, (IV) $R26^{mT}$ CS-30d, (V) $R26^{mT}$ -60d, and (VI) $R26^{mT}$ CS-60d groups, with three mice in each group. The $R26^{mT}$ CS mice were exposed to CS for 14, 30, and 60 days.

Wild-type mice were intratracheally instilled with 60 mL adenovirus (5×10^{10} pfu/mL, Vigene Biosciences, Shangdong, China) to generate lung-specific $Krt15$ knockout (Ad $Krt15$) mice. The mice were divided into (I) WT CS group, (II) Ad $Krt15$ CS group, (III) Ad $Krt15$ CS+SB-3CT group, and then were exposed to CS for 2 months. Mice in the Ad $Krt15$ CS+SB-3CT group were intraperitoneally injected with 50 mg/kg SB-3CT which was dissolved in 10% Dimethyl sulfoxide (HY-Y0320, MCE), 20% Cremophor EL (HY-Y1890, MCE), and 70% ddH₂O every other day for 14 days at 6 weeks after smoke exposure. All mice were housed in animal facilities at Zhongshan Hospital, Fudan University (Shanghai, China). All experimental procedures were approved by the Animal Care and Use Committee of Zhongshan Hospital, Fudan University (No.2022.032).

Hematoxylin and eosin (H&E), Masson and TUNEL staining

The right upper lobes of lung tissues were infiltrated with 4% formaldehyde phosphate buffer for 24 h. The fixed lung tissue was subsequently embedded with paraffin and sectioned into 3 mm sections which were dewaxed by xylene three times and were soaked in 100%, 95%, and 75% alcohol in turn for further staining. For H&E staining, the sections were stained with hematoxylin dye and eosin dye. For masson staining, the sections were stained with hematoxylin for 5 min, then stained with ponceumic red for 10 min and phosphomolybdate for 5 min, and finally stained with aniline blue and differentiated with 1% acetic acid. For TUNEL staining, after the sections being repaired and the membranes being broken, TdT and dUTP were added at 2:29 and incubated at 37 °C for 2 h. Hydrogen peroxide solution (3%) was used to block endogenous peroxidase. After adding converter POD to each section, DAB was added and Harris hematoxylin was re-dyed.

RNA-sequencing analysis

Total RNA was extracted from the lung tissue of the four groups (WT, WT CS, $Krt15^{-/-}$ and $Krt15^{-/-}$ CS) using TRIzol reagent (Thermo Fisher Scientific, Waltham, MA, USA) following the manufacturer's protocol. Sequencing libraries were generated using NEB-Next Ultra™ RNA Library Prep Kit for Illumina (NEB, Houston, TX, USA). The clustering of the index-coded samples was performed on a cBot Cluster Generation System using TruSeq PE Cluster Kit v3-cBot-HS (Illumina, San Diego, CA, USA). RNA-sequencing analysis was performed by Shanghai Genechem Co., Ltd. (Shanghai, China).

Immunofluorescence (IF)

Frozen sections of lung tissue were stained with rabbit anti-Sftpc antibody (1:500; DF6647, Affinity Biosciences, Cincinnati, OH, USA) overnight at 4 °C. Then the sections were incubated for 1 h at 37 °C with Alexa Fluor® 488 goat anti-mouse IgG (H+L) (A11001, ThermoFisher Scientific, Waltham, MA, USA). 4',6-diamidino-2-phenylindole (DAPI, C1006, Beyotime Biotechnology, Shanghai, China) was used to counterstain the nuclei.

Immunohistochemistry (IHC)

After deparaffinization, the right lung lobes of four groups were incubated overnight at 4 °C with $Krt15$ (ab52816, Abcam), E-cadherin (3195T, Cell Signaling Technology, Boston, MA, USA), and Vimentin (5741T, Cell Signaling Technology) antibodies. The following day, sections were stained with horseradish peroxidase-conjugated secondary antibodies for 60 min at room temperature. 3,3'-Diaminobenzidine staining was performed, and the results were observed under a microscope (Olympus, Tokyo, Japan).

Enzyme-linked immunosorbent assay (ELISA)

The contents of MMP-9, IL-6, TNF- α , and IL-1 β in BALF were detected using Mouse MMP9 DuoSet (DY6718, R&D systems, Minneapolis, MN, USA), IL-6 DuoSet (DY406, R&D systems), IL-1 β DuoSet (DY401, R&D systems), and TNF- α DuoSet (DY410, R&D systems) ELISA kits, respectively, following the manufacturer's instructions. The MMP-9 content in the HBE cell supernatant was detected using a DuoSet ELISA kit (DY911-05, R&D Systems) according to the instructions supplied with the kit.

Preparation of cigarette smoke extract (CSE)

Five cigarettes (Daqianmen, Shanghai Tobacco Group Co., Ltd. Shanghai, China) were lightly sucked into

10 mL serum-free cell culture media using a negative pressure aspirator at 6 min/mL. Subsequently, the CSE solution was filtered using 0.22 mm filters (SLGS033SS, Merck Millipore, MA, USA) and stored for further use. The optical density of the CSE (100%) at 320 nm is 4.1.

Cell culture

HBE cells were purchased from the American Type Culture Collection and cultured in RPMI 1640 (Gibco, Carlsbad, CA, USA) containing 10% FBS (Gibco) and 1% penicillin–streptomycin (Gibco) at 37 °C in an incubator containing 5% CO₂. For CSE exposure experiment, HBE cells were stimulated with 0%, 0.5%, and 1.5% CSE for 24 and 48 h.

Lentiviral construction and infection

Lentivirus-containing short hairpin RNA (shRNA) targeting KRT15 and Lentivirus-vectors were pursued by Genechem (Shanghai, China). 5×10^4 HBE cells were incubated in 6-well plates for 24 h in a 5% CO₂ incubator. And the following day, the HBE cells were cultured in 1 mL medium with 5 mg/mL polybrene (Genechem) and a lentivirus-containing shRNA targeting KRT15 (shKRT15) or lentivirus-vectors (negative control). After incubating for 24 h, the medium was replaced with a fresh normal medium. These cells were divided into four groups based on their CSE and Lentivirus regimes: (I) Negative control (NC), (II) NC CSE, (III) shKRT15, (IV) shKRT15 CSE. The cells in NC CSE and shKRT15 CSE group were stimulated by 1.5% CSE for 48 h.

Quantitative real-time-PCR (qRT-PCR)

RNA was extracted from lung tissue using RNA-Quick Purification Kit (RN001, Shanghai Yishan Biotechnology Co. Ltd., Shanghai, China) and was reverse-transcribed into cDNA using PrimeScript™ RT reagent kit (RR037A, Takara Biotechnology, Osaka, Japan). qRT-PCR was performed to amplify the target genes (RR420A, Takara Biotechnology). The primer sequences are shown in Table 1.

Table 1 Primers used for quantitative real-time-PCR

Gene	Sequence(5' → 3')
Mouse Krt15 forward	AGCTATTGCAGAGAAAAACCGT
Mouse Krt15 reverse	GGTCCGTCTCAGGTCGTGTG
Human KRT15 forward	TCTGCTAGGTTTGTCTCTTCAGG
Human KRT15 reverse	CCAGGGCACGTACCTTGTG
Human MMP-9 forward	AGACCTGGGCAGATCCAAAC
Human MMP-9 reverse	CGGCAAGTCTTCCGAGTAGT

Krt15 Keratin 15, *MMP-9* Matrix metalloproteinase-9

Cell viability assay

Approximately 1×10^4 cells per well were seeded into 96-well plates and cultured for 24 h. At indicated time points (24 and 48 h), the medium in every well was replaced by new medium containing 10% CCK-8 solution (40203, Yeasen, Shanghai, China), and the plates were incubated for 1 h. Then the absorbance values at 460 nm were measured by FlexStation3 Multi-Mode Microplate Readers.

Western blot analysis

The lung tissue was lysed by RIPA (P0013B, Beyotime Biotechnology, Shanghai, China) to obtain the protein. After the protein concentration of the right lung was measured using a spectrometer (NanoDrop 2000, Thermo Fisher Scientific, Waltham, MA, USA), the protein was first separated using sodium dodecyl-sulfate polyacrylamide gel electrophoresis, transformed into polyvinylidene difluoride membranes, and then blocked using QuickBlock™ Blocking Buffer (P0231, Beyotime Biotechnology). The polyvinylidene difluoride membranes were then stained with Krt15 (ab52816, Abcam), E-cadherin (3195T, Cell Signaling Technology), or Vimentin (5741T, Cell Signaling Technology) antibodies at 4 °C overnight. The following day, rabbit peroxidase-conjugated secondary antibodies (7074P2, Cell Signaling Technology) were used to detect target proteins.

Statistical analysis

All data analyses were performed using GraphPad Prism9.0 software. A one-way analysis of variance was used for multiple group comparisons. All results are shown as the mean ± standard deviation (SD). Statistical significance was set at $p < 0.05$.

KRT15 is overexpressed in patients with COPD and CS-exposed mice

Estimation of the KRT15 expression in the two GEO datasets (GSE5058 and GSE8545) revealed a higher expression in patients with COPD (N=33) than that in nonsmokers (N=23) ($p < 0.01$; Fig. 1A and B).

To investigate the dynamic changes in Krt15⁺ cells following CS treatment in vivo, we used *Krt15-CrePGR;Rosa26-LSL-tdTomato* reporter mice to track Krt15⁺ cells [25, 27]. The intensity of Tomato⁺ (Krt15⁺) cells in the bronchial epithelial cells significantly increased in *Krt15-CrePGR;Rosa26-LSL-tdTomato* mice exposed to CS (on days 14, 30, and 60) compared to that in those not exposed to CS in exposure-duration dependent manner (Fig. 1C and D). Krt15⁺ cells in WT and WT

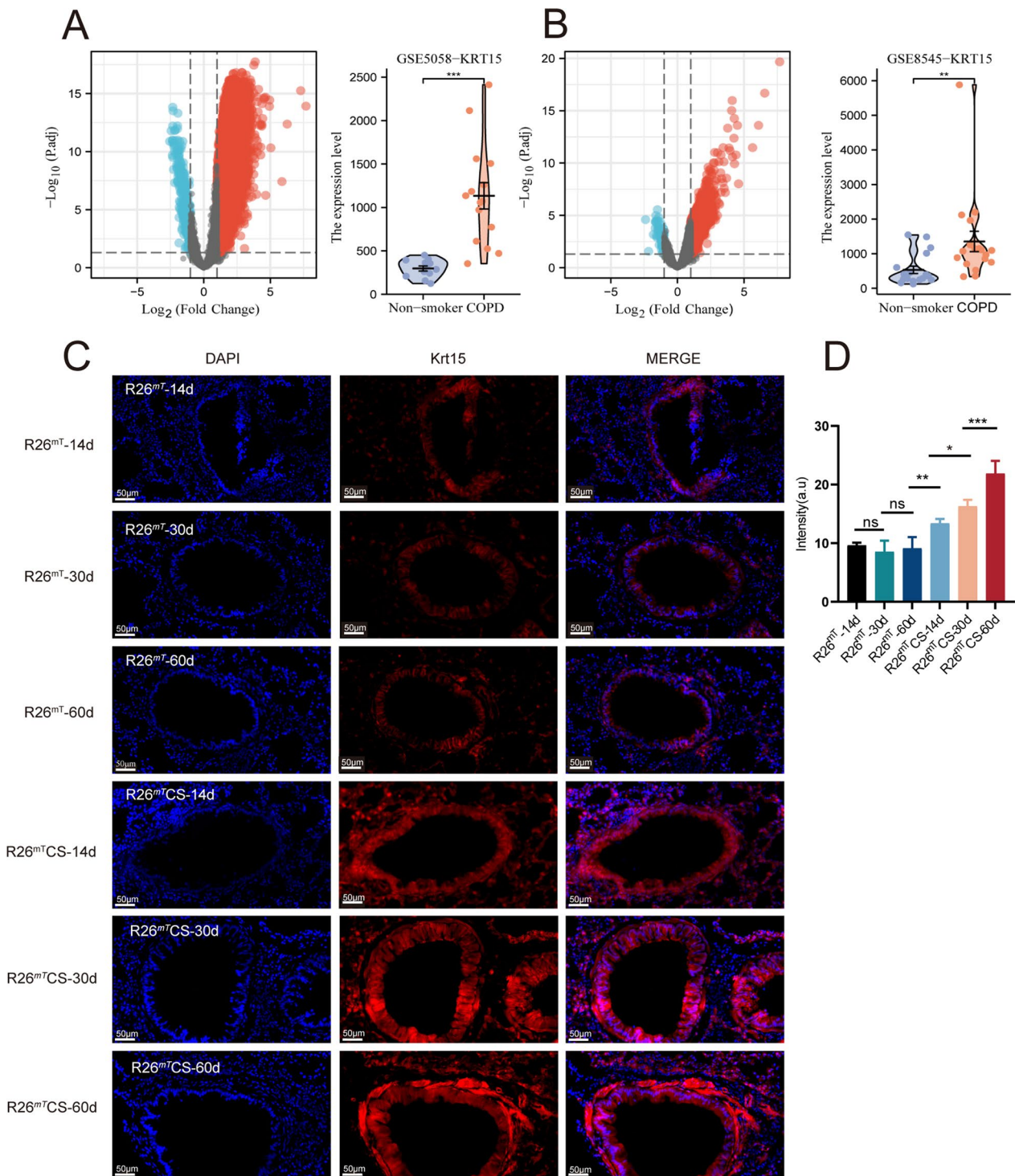


Fig. 1 Expression of Krt15 in humans and mice. **A** and **B** Comparison of expression of Krt15 in nonsmokers and patients with COPD in GSE5058 and GSE8545 datasets obtained from the Gene Expression Omnibus database. **C** Immunofluorescence intensity of Tomato⁺ (Krt15⁺) cells (Red) in *Krt15-CrePGR;Rosa26-LSL-tdTomato* reporter mice; 4,6-diamidino-2-phenylindole (DAPI) was used to stain nuclei. **D** The intensity of Krt15⁺; N=3 in each group.**p* < 0.05; ***p* < 0.01; ****p* < 0.001. R26^{mt}-14d, R26^{mt}-30d, R26^{mt}-60d, *Krt15-CrePGR;Rosa26-LSL-tdTomato* mice exposed to air on days 14, 30, and 60; R26^{mt}CS-14d, R26^{mt}CS-30d, R26^{mt}CS-60d, *Krt15-CrePGR;Rosa26-LSL-tdTomato* mice exposed to CS (on days 14, 30, and 60)

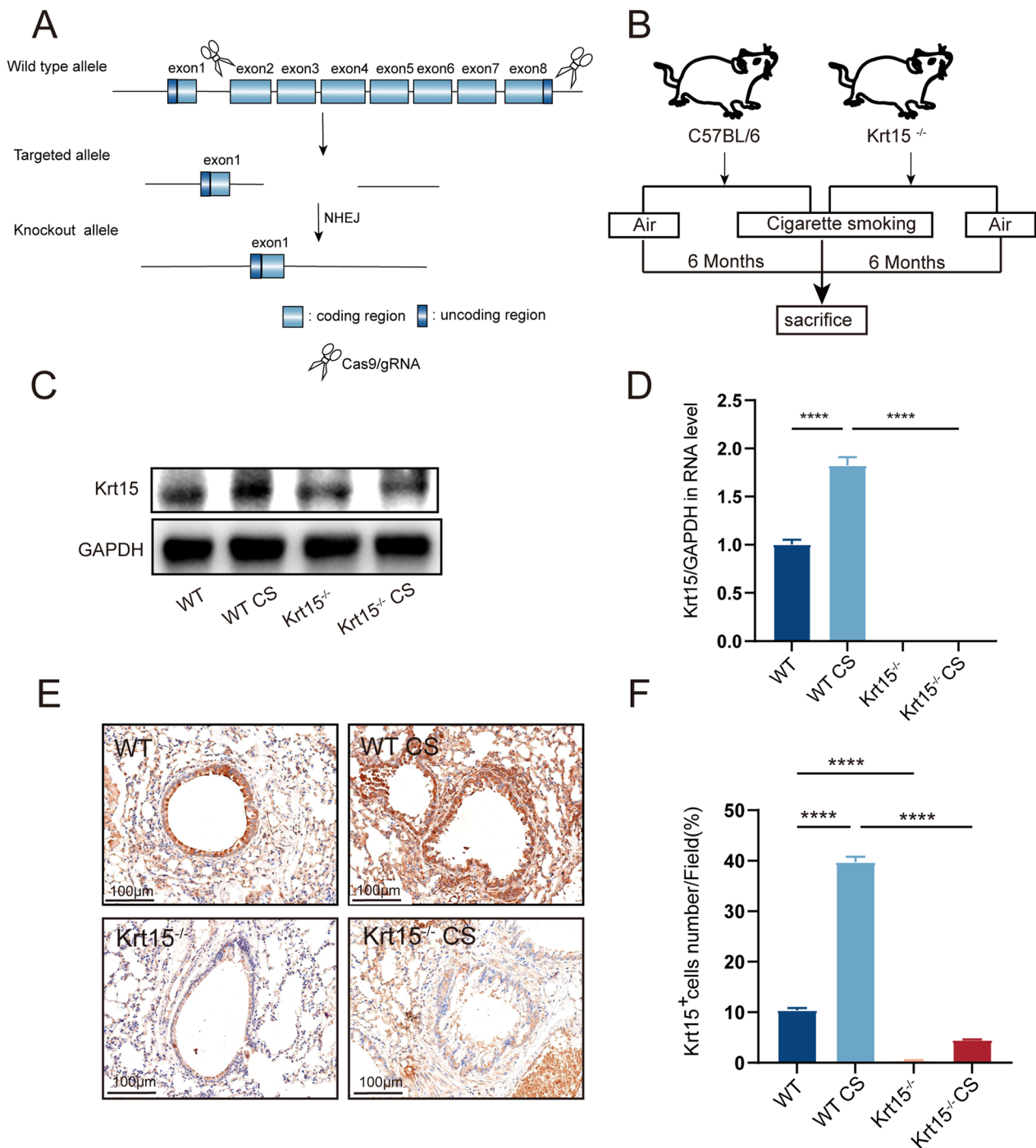


Fig. 2 CRISPR/Cas9 gene editing technology to generate Krt15 knockout mice. **A** Schematic diagram of CRISPR/Cas9 gene editing to knockout *Krt15*. **B** Scheme of the establishment of mice COPD model by exposing WT CS and Krt15^{-/-} CS mice to cigarette smoking for six months, while the WT and Krt15^{-/-} mice were exposed to air for six months. **C**, **D** Expression of Krt15. **C** protein detected using western blot and **D** mRNA detected using qRT-PCR in the four groups; GAPDH was used as the internal control. **E** Immunohistochemistry (IHC) analysis of Krt15. N=6 in each group. **F** Percentage of Krt15⁺ cells in IHC. *****p* < 0.0001. WT wild-type, WT CS wild-type + CS exposure, Krt15^{-/-} Krt15 knockout mice, Krt15^{-/-} CS Krt15 knockout mice + CS exposure, CS cigarette smoking

CS groups did not show autofluorescence (Additional file 1: Figure S1).

Knockout of Krt15 aggravates lung injury in CS-exposed mice

To investigate the role of Krt15 in COPD, the *Krt15*^{-/-} mice generated using the CRISPR-Cas9 (Fig. 2A) were

exposed to CS for six months to establish a COPD model (Fig. 2B). The qRT-PCR and western blot results demonstrated that Krt15 mRNA and protein expression increased after CS exposure in the WT CS group compared to that in the WT group. In contrast, they were almost completely absent in the *Krt15*^{-/-} and *Krt15*^{-/-} CS groups (Fig. 2C and D). Consistent with this, IHC

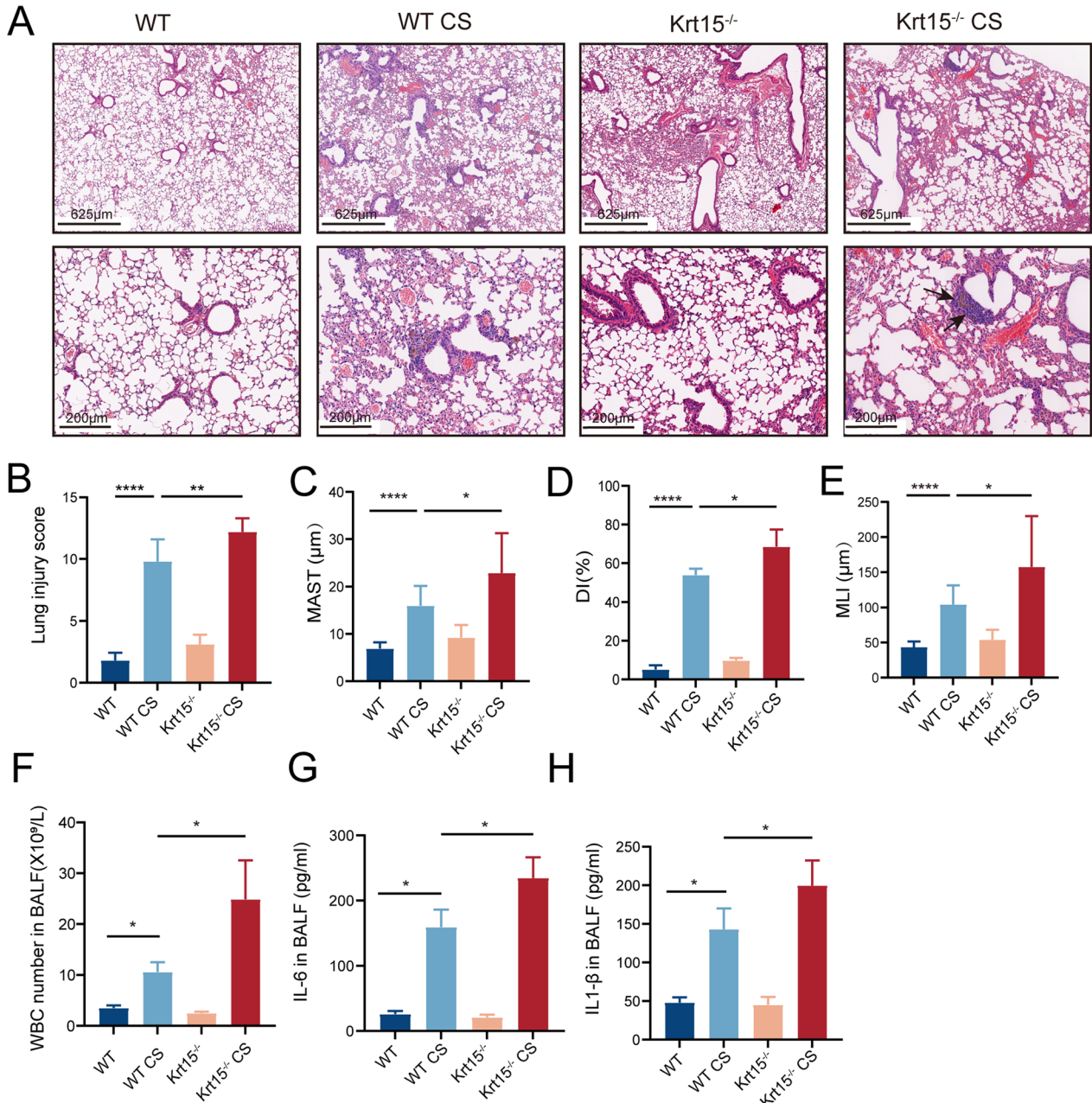


Fig. 3 Knockout of Krt15 aggravates CS-induced lung injury and inflammatory infiltration. **A** H&E staining, **B** lung injury score, **C** MAST, **D** DI, **E** MLI, **F** WBC number in BALF, and **G** IL-6 and IL-1β (**H**) concentration. **p* < 0.05; ***p* < 0.01; ****p* < 0.001; *****p* < 0.0001. WT wild-type, WT CS wild-type + CS exposure, *Krt15*^{-/-} *Krt15* knockout mice, *Krt15*^{-/-} CS *Krt15* knockout mice + CS exposure, CS cigarette smoking. The arrows point to inducible bronchus-associated lymphoid tissue (iBALT)

results showed that *Krt15* expression increased after CS and decreased in the *Krt15*^{-/-} and *Krt15*^{-/-} CS groups (Fig. 2E and F).

H&E staining demonstrated more leukocyte infiltration, indicating higher inducible bronchus-associated lymphoid tissue (iBALT) in the WT CS group than that in the WT group, which was further increased in *Krt15*^{-/-} CS group (Fig. 3A). Subsequently, we evaluated the lung injury score [29], which revealed significantly higher lung injury scores in the *Krt15*^{-/-} CS group than those in the WT CS group ($p < 0.01$; Fig. 3B). Furthermore, the deficiency of *Krt15* resulted in the thickening of the alveolar walls and airspace enlargement. The thickness of alveolar walls (mean alveolar septal thickness), percentage of destructive alveoli (destructive index), and mean linear intercept (MLI) [28, 30], were significantly increased in the WT CS group compared to those in the WT group, and further increased in the *Krt15*^{-/-} CS group (Fig. 3C–E). Moreover, the number of white blood cells and the secretion of IL-6 and IL-1 β in BALF were significantly increased in the WT CS group compared to those in the WT group ($p < 0.05$ in all cases) and further increased in the *Krt15*^{-/-} CS group compared to those in the WT CS group ($p < 0.05$ in all cases) (Fig. 3F–H).

Extracellular matrix plays a key role in *Krt15*-mediated regulation of COPD

To investigate the specific mechanisms of *Krt15* in the development and occurrence of COPD, we performed RNA sequencing. The Venn plot revealed that 1176 genes were upregulated in the WT CS group compared to those in the WT group. Among these genes, 66 genes were further upregulated in the *Krt15*^{-/-} CS group in comparison with WT CS group (Fig. 4A). Moreover, 1300 genes were downregulated in WT CS group compared to those in the WT group. Among these genes, 48 genes were further downregulated in the *Krt15*^{-/-} CS group in comparison with WT CS group (Fig. 4B). Kyoto Encyclopedia of Genes and Genomes (KEGG) analysis of these differentially expressed genes identified the enrichment of the cell adhesion molecules (CAMs) and ECM-receptor interaction pathways (Fig. 4C). Gene Ontology (GO) analysis showed that the genes were enriched in cell–cell junctions and extracellular matrix structural constituents (Fig. 4D). Figure 4F shows a heatmap of some of the top differentially expressed genes.

Krt15 regulates the EMT progression by promoting MMP-9 expression

Based on the RNA sequencing analysis, we next explored the effect of *Krt15* on EMT. Masson staining demonstrated that CS exposure for 6 months led to the development of a typical airway remodeling phenotype with

significant collagen disposition and airway thickening in WT mice, which was further worsened in the absence of *Krt15* (Fig. 5A). E-cadherin is often selected as a marker of the epithelium and Vimentin as a marker of the mesenchyme. IHC revealed that *Krt15* knockout reduced the expression of E-cadherin and increased that of Vimentin in the *Krt15*^{-/-} CS group compared with those in the WT CS group (Fig. 5A–C). These results were consistent with the protein expression of E-cadherin and Vimentin measured using western blot (Fig. 5D).

CS induces MMP-9 release, which has been shown to play a key role in EMT progression [31–33]. Therefore, we used ELISA to measure MMP-9 concentration in BALF. The results demonstrated that CS promoted MMP-9 expression, which was further increased by *Krt15* knockout (Fig. 5E). To validate whether MMP9 mediates the role of *Krt15* in the pathogenesis of COPD, we then generated lung-specific *Krt15* knockout (Ad*Krt15*) mice by intratracheally instilled with adenovirus. After intraperitoneal injection of SB-3CT, an MMP-9 inhibitor, for two weeks, it was found that mice in the Ad*Krt15* CS+SB-3CT group showed less airway remodeling and destruction of alveolar walls than those in the Ad*Krt15* CS group (Fig. 6A). Compared with Ad*Krt15* CS group, the expression of E-cadherin was increased while the expression of Vimentin was decreased in Ad*Krt15* CS+SB-3CT group (Fig. 6A). At the same time, SB-3CT could inhibit the release of inflammatory cytokines IL-6, TNF- α and IL-1 β (Fig. 6B–D). The above results suggest that *Krt15* regulates EMT progression by promoting MMP-9.

KRT15 knockdown promotes MMP-9 expression and EMT progression in vitro

To confirm the role of *KRT15* in vitro, HBE cells were stimulated with CSE to construct an in vitro COPD model. We first examined the mRNA expression of *KRT15* at different time points and concentrations of CSE in HBE cells and found that CSE promoted the expression of *KRT15* in a concentration- and time-dependent manner (Fig. 7A and B). HBE cells were exposed to 1.5% CSE for 48 h for subsequent experiments. Subsequently, we knocked down *KRT15* in HBE cells using a shRNA targeting *KRT15* (Fig. 7C). CCK-8 assay showed that the knockdown of *KRT15* reduced cell viability in the sh*KRT15* CSE group compared to that in the NC CSE group at different time points (Fig. 7D).

Furthermore, western blotting to evaluate the EMT process in vitro revealed that *KRT15* knockdown reduced the expression of E-cadherin and increased that of Vimentin in the sh*KRT15* CSE group compared to those in the NC CSE group (Fig. 8A). qRT-PCR and ELISA results demonstrated increased *Mmp9* mRNA and protein expression in the NC CSE group

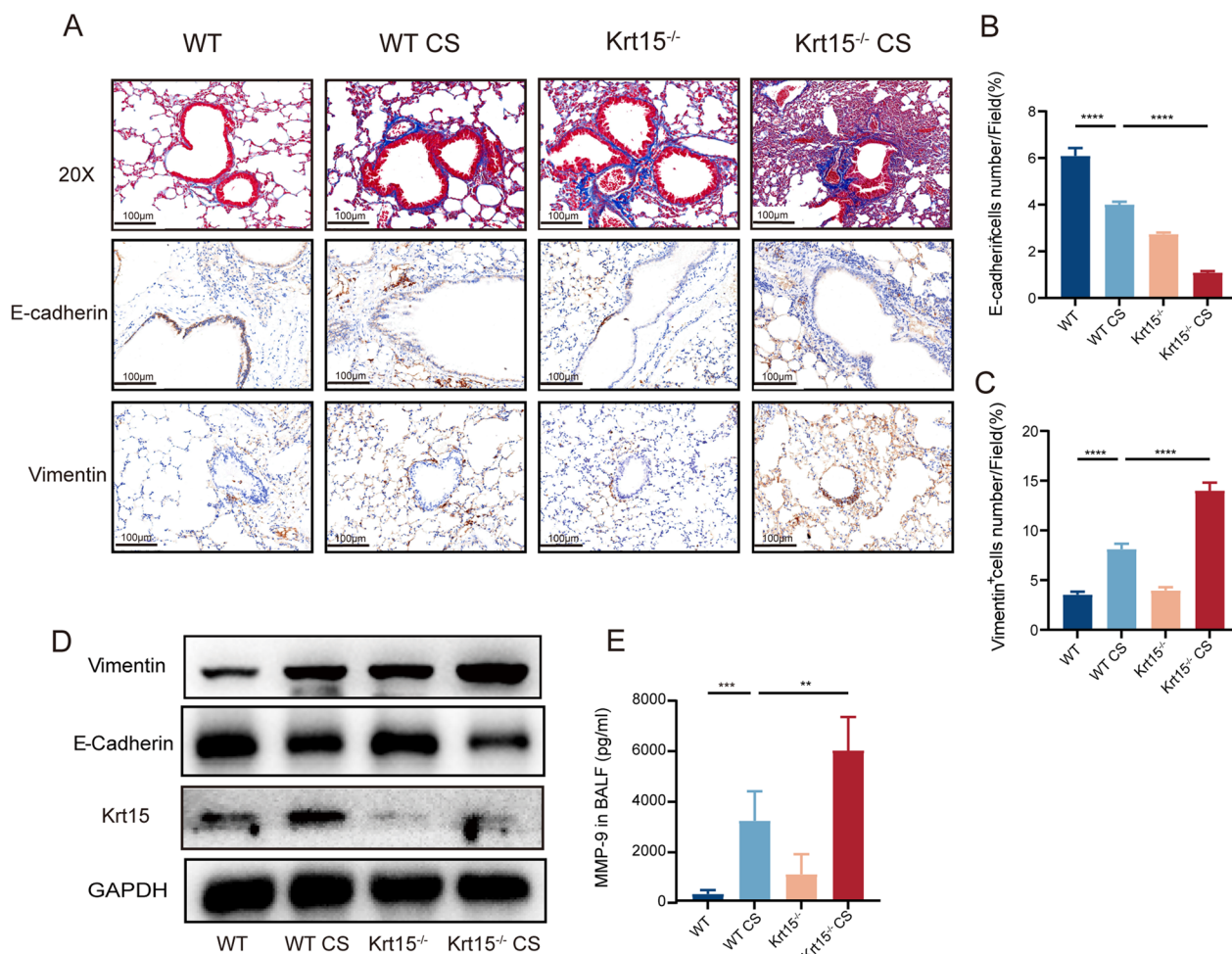


Fig. 5 Krt15 regulates the EMT progression. **A** Masson staining and immunohistochemistry of E-cadherin and Vimentin. **B** and **C** expression of E-cadherin and Vimentin in IHC. **D** western blot analysis of Krt15, E-cadherin, and Vimentin. **E** MMP-9 concentration in BALF(pg/mL); ** $p < 0.01$; *** $p < 0.001$

immunofluorescence experiments to double-stain Krt15 and Sftpc, a marker of AT2 cells. CS exposure increased the number of Tomato⁺ (Krt15⁺)/Sftpc⁺ cells in *Krt15-CrePGR; Rosa26-LSL-tdTomato* mice on days 14, 30, and 60 compared to that without CS exposure on day 60 (Fig. 9B and C). Furthermore, the TUNEL staining assessment showed that there were more apoptotic cells in the alveoli of Krt15^{-/-} CS group than those of WT CS group (Fig. 9D and E).

Discussion

COPD is an irreversible disease characterized by airway remodeling and accelerated decline in lung function [34–36], which significantly affects the quality of life in patients and increases economic and social burden worldwide [6]. Although it is one of the leading causes of death, the existing treatment methods are limited and can mainly alleviate the clinical symptoms of COPD.

None of the current treatment methods are efficient in improving lung function and mortality in patients with COPD [5, 37, 38]. Therefore, identifying the endogenous regeneration mechanisms that can restore the decline in lung function is important to treat COPD [39]. KRT15 identified as a stem cell marker in hair follicles [40], has gained recognition in identifying long-lived progenitor cells in the esophageal epithelium and small intestine crypts [20, 25]. Moreover, a recent study has demonstrated its potential role in airway basal cells to compensate for the lack of Krt14 that forms the intermediate filaments for establishing the basal epithelial cytoskeleton [26]. In this study, we explored the potential role of Krt15 in COPD and its underlying molecular mechanisms.

Our findings revealed a significantly higher expression of KRT15 in patients with COPD than that in nonsmokers. We also showed for the first time that Krt15⁺ cells were mainly expressed in the bronchial epithelium, and

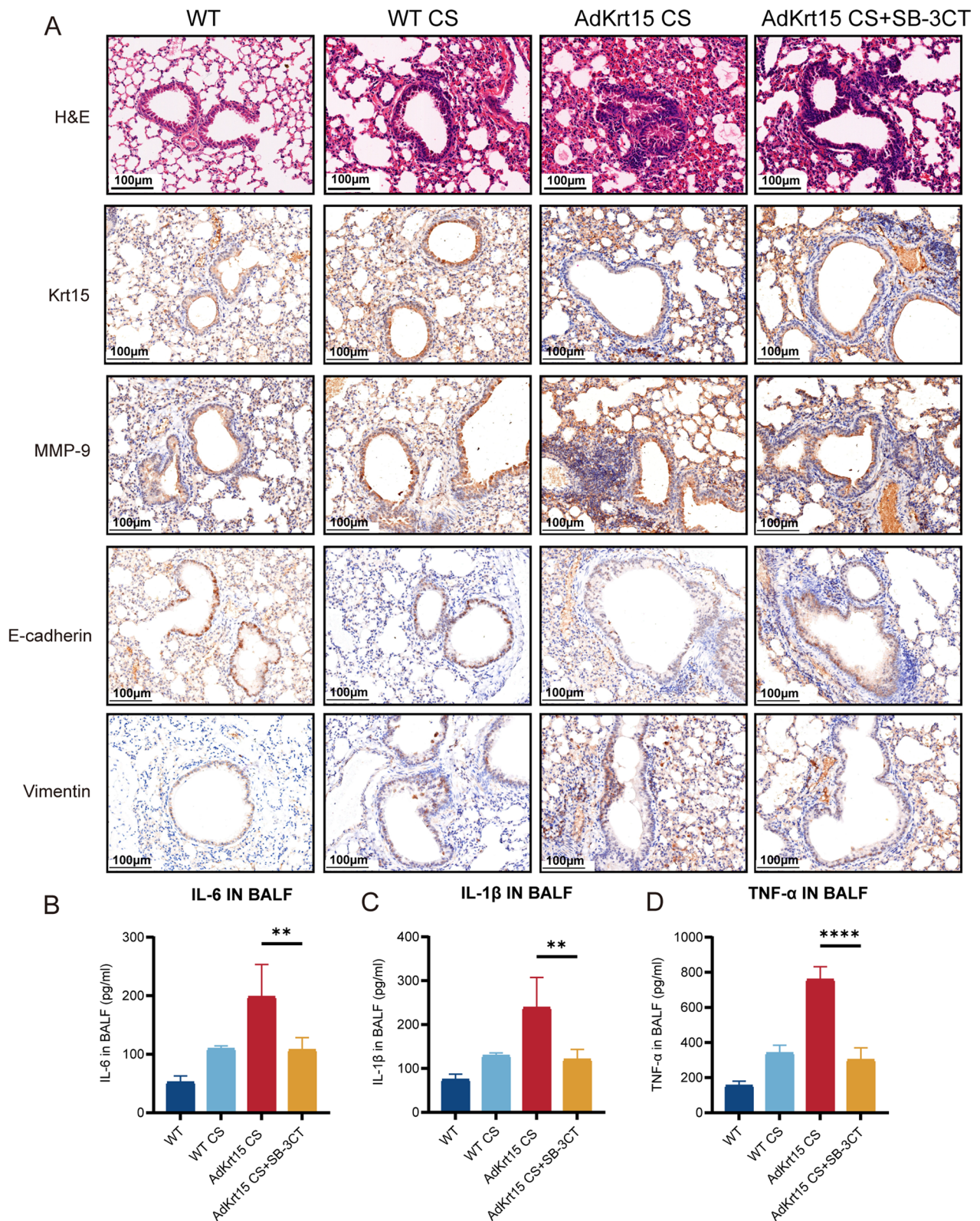


Fig. 6 Inhibition of MMP9 alleviated the exacerbation of lung injury and inflammation caused by Krt15 knockdown in CS-exposed mice. **A** H&E and IHC stainings of Krt15, MMP-9, E-cadherin, and Vimentin. **B** The concentration of IL-6 (**B**); IL-1β (**C**); and TNF-α (**D**) in BALF. ** $p < 0.01$, **** $p < 0.0001$. WT wild-type, WT CS wild-type mice + CS exposure, AdKrt15 CS wild-type mice + 60 mL adenovirus (5×10^{10} pfu/mL) + CS, AdKrt15 CS + SB-3CT wild-type mice + 60 mL adenovirus + CS + SB-3CT, CS cigarette smoking, SB-3CT an inhibitor of MMP-9

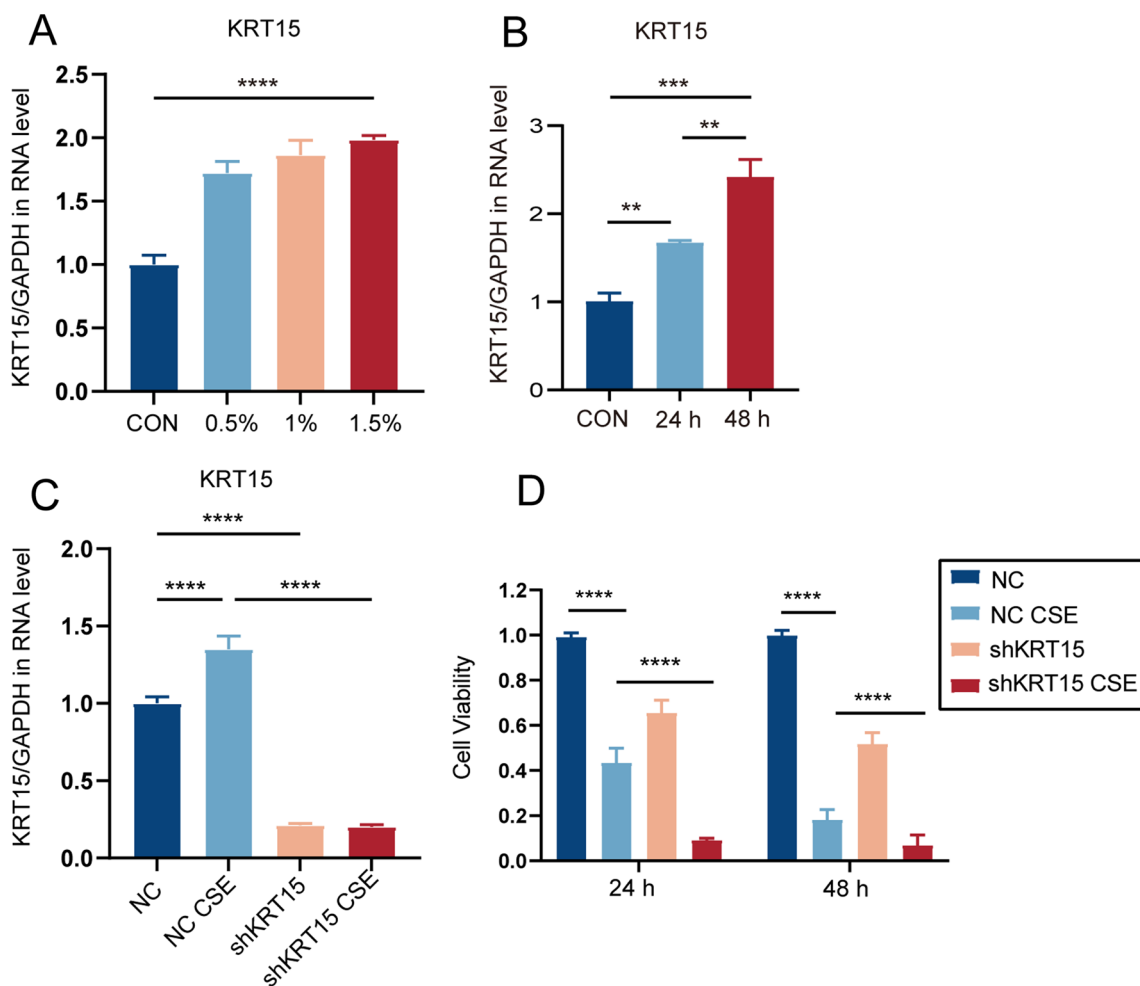


Fig. 7 CSE stimulated Krt15 mRNA expression and reduced cell viability. **A** stimulated with 0.5%, 1%, and 1.5% CSE for 48 h, **B** with 1.5% CSE for 24 and 48 h, **C** treated with or without shRNA targeting KRT15 in the presence or absence of CSE. **D** Viability of HBE cells treated with or without shRNA targeting KRT15 in the presence or absence of CSE. *** $p < 0.001$, **** $p < 0.0001$. NC negative control, NC CSE negative control + 1.5% CSE, shKRT15 HBE cells using an shRNA targeting KRT15; shKRT15 CSE, HBE cells using an shRNA targeting KRT15 + 1.5% CSE

their expression increased with an increase in CS exposure time. In addition, both mRNA and protein expression of Krt15 in the lung tissues of mice significantly increased after exposure to CS. In addition, after stimulating HBE cells with CSE, KRT15 expression significantly increased in a time- and concentration-dependent manner. These results suggest that Krt15 plays an important role in the occurrence and development of COPD.

Furthermore, CS exposure for six months accelerated the severity of lung injury in Krt15^{-/-} mice and more significant tertiary lymphoid structure formation was observed in iBALT [41]. iBALT can cause the recruitment of inflammatory cells and the destruction of alveolar walls that is related to emphysema during chronic CS exposure [38, 42–44]. In consistent with this, the

highest percentage of alveolar destruction and secretion of inflammatory cytokines IL-6 and IL-1 β was in the Krt15^{-/-} CS group (Fig. 3G and H).

Next, we assessed the degree of emphysema by measuring MLI in the four groups [45]. After exposure to CS for six months, the MLI in the Krt15^{-/-} CS group was higher than that in the WT CS group. In the Krt15⁺ cell-tracing experiment, the number of Tomato⁺(Krt15⁺)/Sftpc⁺ cells increased significantly with increased CS exposure time. Sftpc is often used as a marker for AT2 cells [46, 47], which act as stem cells during lung injury [48]. Prolonged exposure to CS disposes of AT2 cells to senescence and apoptosis [49, 50], consequently leading to failure in alveolar wall maintenance, which results in emphysema and hinders the damage repair [51]. Previous

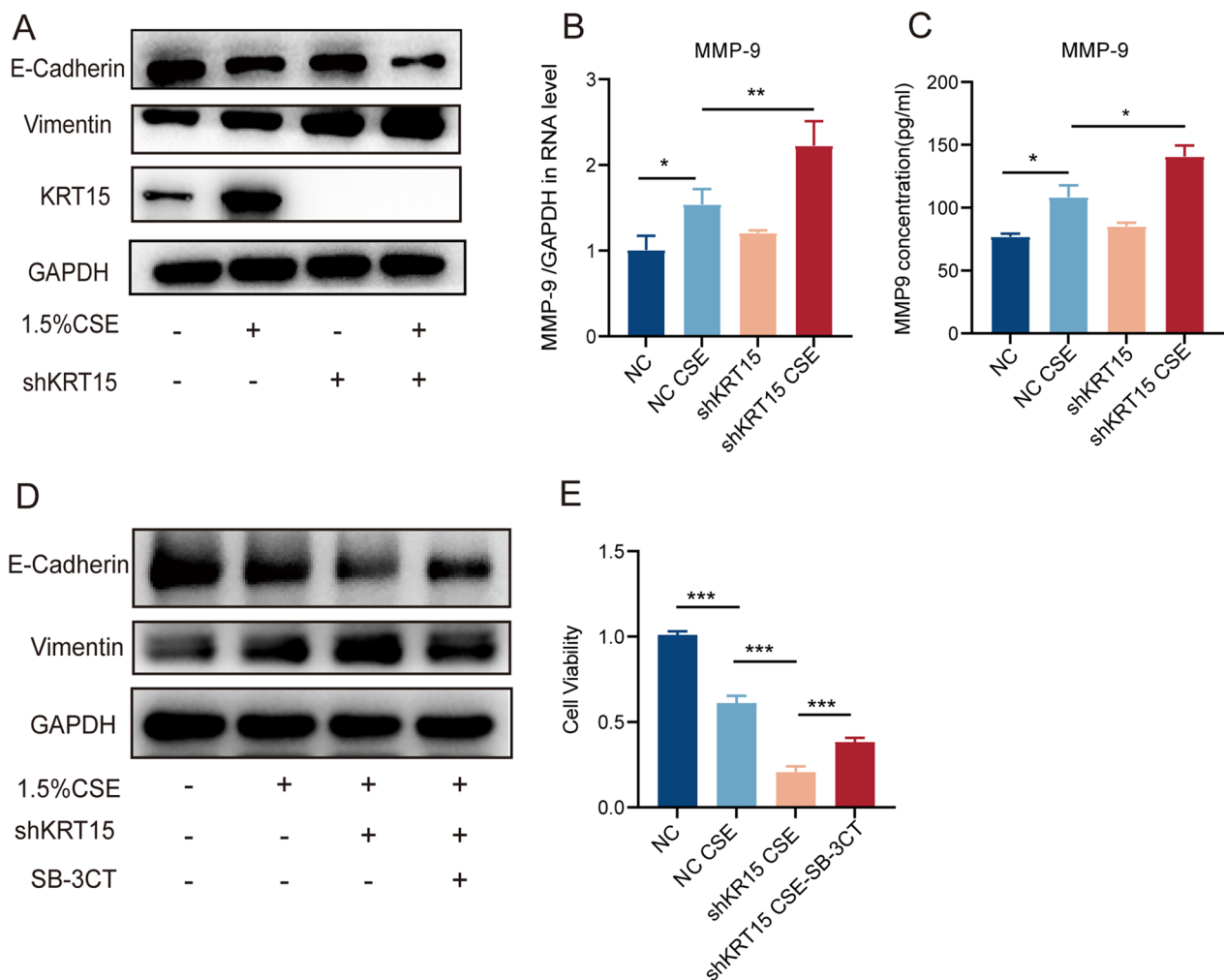


Fig. 8 KRT15 knockdown promoted MMP-9 expression and EMT progression in vitro. **A** Western blot analysis of E-cadherin and Vimentin. **B** mRNA level of MMP-9 in HBE cells. **C** MMP-9 concentration in cellular supernatant. **D** Protein levels of E-cadherin and Vimentin. **E** Cell viability. * $p < 0.05$; ** $p < 0.01$; *** $p < 0.001$. NC negative control, NC CSE negative control + 1.5% CSE, shKRT15 HBE cells using an shRNA targeting KRT15, shKRT15 CSE HBE cells using an shRNA targeting KRT15 + 1.5% CSE, shKRT15 CSE-SB-3CT HBE cells using an shRNA targeting KRT15 + 1.5% CSE + SB-3CT

studies have demonstrated that the stemness of AT2 cells increases to defend against CS-induced lung injury, but fail to compensate the damage of AT2 cells and avoid emphysema [52]. Furthermore, TUNEL staining identified an increased number of apoptotic cells in the alveolar region in the *Krt15^{-/-}* CS group compared to the WT CS group in this study. These results indicate that *Krt15* plays a vital role in protecting alveoli.

Conversely, the results of RNA-sequencing analysis suggest that the role of *Krt15* in COPD is related to the structural constituents of the extracellular matrix. Both IHC and western blot results demonstrated that CS exposure decreased the expression of E-cadherin and increased that of Vimentin in *Krt15* knockout mice. Because E-cadherin and Vimentin play key roles in EMT

[9], we inferred that *Krt15* knockout leads to increased airway remodeling in mice by promoting EMT progression. The in vitro experiments confirmed these in vivo results. After CSE stimulation, shKRT15 cells exhibited higher Vimentin expression, lower E-cadherin expression, and decreased cell viability.

CSE and CS can stimulate the expression of MMP-9 [31, 53, 54], and multiple studies have shown that MMP-9 is highly correlated with EMT processes. Recombinant MMP-9 induces EMT in the lung epithelium and glomerular endothelium [32, 55]. We demonstrated that *Krt15^{-/-}* mice and shKRT15 cells secreted more MMP-9 upon stimulation with CSE and CS, respectively. Furthermore, SB-3CT reversed the CSE-induced alterations in E-cadherin and Vimentin expression and increased cell

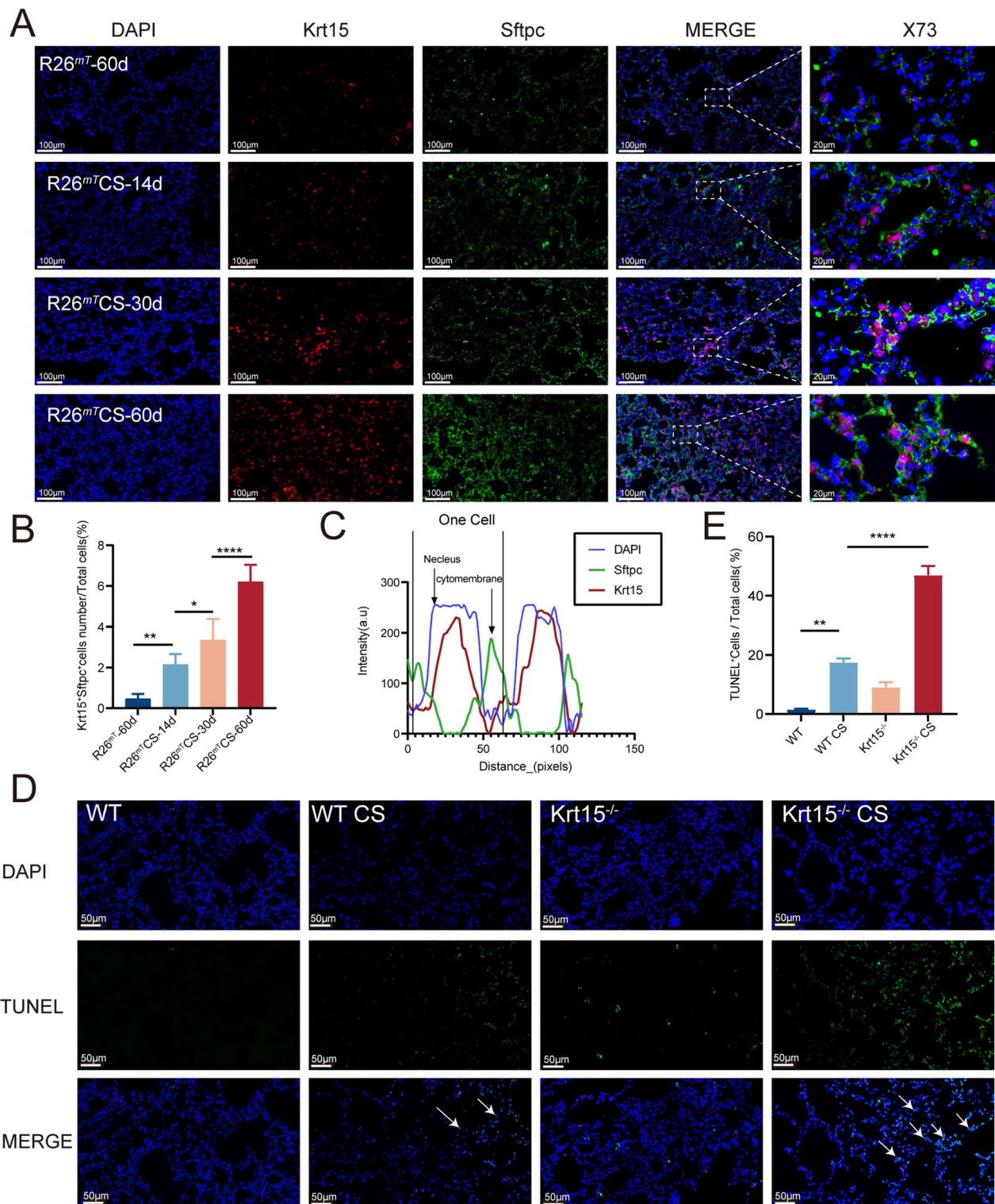


Fig. 9 Krt15⁺ cells transform into AT2 cells to protect alveoli. **A** Immunofluorescence staining of lung tissue with Krt15 (Red) and Sftpc (Green). **B** The ratio of Krt15⁺Sftpc⁺ cells/Total cells. **C** Staining-intensity profiles showing signals from three fluorescent channels. **D** The ratio of TUNEL⁺ cells/Total cells. **E** TUNEL staining. N = 3 in each group. **p* < 0.05; ***p* < 0.01; ****p* < 0.001; *****p* < 0.0001. R26^{mT}-60d, *Krt15-CrePGR; Rosa26-LSL-tdTomato* mice exposed to air on days 60; R26^{mT}CS-14d, R26^{mT}CS-30d R26^{mT}CS-60d, *Krt15-CrePGR; Rosa26-LSL-tdTomato* mice exposed to CS (on days 14, 30, and 60). *WT* wild-type, *WT CS* wild-type + CS exposure, *Krt15^{-/-}* *Krt15* knockout mice, *Krt15^{-/-} CS* *Krt15* knockout mice + CS exposure, *CS* cigarette smoking. The arrows point to TUNEL⁺ cells

viability. These results prove that silencing of Krt15 promotes EMT by upregulating the expression of MMP-9.

Conclusion

Here, we established the mice models of COPD and unraveled the potential role of Krt15 in COPD and its underlying molecular mechanisms. The findings of the present study demonstrate that Krt15 negatively regulates EMT by promoting MMP-9 expression and protecting alveoli structure. Overall, these findings suggest Krt15 is an important target for COPD treatment.

Abbreviations

Krt15	Keratin15
COPD	Chronic obstructive pulmonary disease
CS	Cigarette smoking
WT	Wild-type
HBE	Human bronchial epithelial
CSE	Cigarette smoke extract
MMP-9	Matrix metalloproteinase-9
EMT	Epithelial–mesenchymal transformation
iBALT	Inducible bronchus-associated lymphoid tissue

Supplementary Information

The online version contains supplementary material available at <https://doi.org/10.1186/s12931-023-02598-w>.

Additional file 1: Figure S1. Krt15⁺ cells did not show autofluorescence. WT, wild-type; WT CS, wild-type + CS exposure of 60 days.

Author contributions

WZ: performed experiments (lead); writing—original draft (lead); data analysis (lead). LH: performed experiments (equal); data analysis (equal). YW: performed experiments (equal); data analysis (equal). LT: data analysis (equal). LH: data analysis (equal). QW: data analysis (equal). YY: data analysis (equal). TP: data analysis (equal). JS: data analysis (equal). YS: Conceptualization (supporting); writing—original draft (supporting). YS: Conceptualization (supporting); writing—original draft (supporting). QZ: Conceptualization (supporting); writing—original draft (supporting). JZ: Conceptualization (supporting); writing—original draft (supporting). All authors reviewed the manuscript.

Funding

This work was supported by National Key Research and Development Program of China (2022YFA0806200), National Natural Science Foundation of China (82070045, 82270040, 82170088), Shanghai Municipal Science and Technology Major Project (ZD2021CY001), Shanghai Municipal Key Clinical Specialty (shslczdk02201), Science and Technology Commission of Shanghai Municipality (20DZ2254400, 20DZ2261200, 21DZ2200600), Natural Science Foundation of Shanghai (20Z11901004), Shanghai Jinshan Municipal Health Commission (GWV-10.1-XK26, JSZK2019A01), Science and Technology Development Fund of Shanghai Pudong New Area (PK2021-Y35), Shanghai Pudong Hospital and the Discipline Construction Promoting Project of Shanghai Pudong Hospital (Zdzk2020 11), and Project of Shanghai Pudong Hospital (RHJJ2017-03).

Availability of data and materials

Not applicable.

Declarations

Ethics approval and consent to participate

All animal experiments were approved by the Animal Care and Use Committee of Zhongshan Hospital, Fudan University (No.2022-032).

Competing interests

The authors report no conflicts of interest in this work.

Author details

¹Department of Pulmonary and Critical Care Medicine, Shanghai Respiratory Research Institute, Zhongshan Hospital, Fudan University, 180 Fenglin Rd, Shanghai 200032, China. ²Department of Respiratory and Critical Care Medicine, Shanghai Pudong Hospital, 2800 Gongwei Rd, Shanghai 201399, China. ³Shanghai Institute of Infectious Disease and Biosecurity, Fudan University, Shanghai 200032, China. ⁴Shanghai Engineering Research Center of Internet of Things for Respiratory Medicine, 180 Fenglin Road, Shanghai 200032, China. ⁵Shanghai Key Laboratory of Lung Inflammation and Injury, 180 Fenglin Road, Shanghai 200032, China. ⁶Department of Thoracic Surgery, Zhongshan Hospital, Fudan University, 180 Fenglin Road, Shanghai 200032, China. ⁷Research Center for Chemical Injury, Emergency and Critical Medicine of Fudan University, Fudan University, Shanghai 200540, China. ⁸Center of Emergency and Critical Medicine in Jinshan Hospital of Fudan University, Fudan University, Shanghai 200540, China. ⁹Key Laboratory of Chemical Injury, Emergency and Critical Medicine of Shanghai Municipal Health Commission, Shanghai 200540, China.

Received: 4 May 2023 Accepted: 7 November 2023

Published online: 25 November 2023

References

- Safiri S, Carson-Chahhoud K, Noori M, et al. Burden of chronic obstructive pulmonary disease and its attributable risk factors in 204 countries and territories, 1990–2019: results from the Global Burden of Disease Study 2019. *BMJ*. 2022;378: e069679.
- Lareau SC, Fahy B, Meek P, Wang A. Chronic obstructive pulmonary disease (COPD). *Am J Respir Crit Care Med*. 2019;199:1–2.
- Burgel PR, Bourdin A, Chanez P, et al. Update on the roles of distal airways in COPD. *Eur Respir Rev*. 2011;20:7–22.
- Chan SMH, Selemidis S, Bozinovski S, Vlahos R. Pathobiological mechanisms underlying metabolic syndrome (MetS) in chronic obstructive pulmonary disease (COPD): clinical significance and therapeutic strategies. *Pharmacol Ther*. 2019;198:160–88.
- Ferrera MC, Labaki WW, Han MK. Advances in chronic obstructive pulmonary disease. *Annu Rev Med*. 2021;72:119–34.
- Adeloye D, Song P, Zhu Y, Campbell H, Sheikh A, Rudan I. Global, regional, and national prevalence of, and risk factors for, chronic obstructive pulmonary disease (COPD) in 2019: a systematic review and modelling analysis. *Lancet Respir Med*. 2022;10:447–58.
- McDonough JE, Yuan R, Suzuki M, et al. Small-airway obstruction and emphysema in chronic obstructive pulmonary disease. *N Engl J Med*. 2011;365:1567–75.
- Kalluri R, Weinberg RA. The basics of epithelial–mesenchymal transition. *J Clin Invest*. 2009;119:1420–8.
- Gohy ST, Hupin C, Fregimilicka C, et al. Imprinting of the COPD airway epithelium for dedifferentiation and mesenchymal transition. *Eur Respir J*. 2015;45:1258–72.
- Lai T, Li Y, Chen M, et al. Heparin-binding epidermal growth factor contributes to COPD disease severity by modulating airway fibrosis and pulmonary epithelial–mesenchymal transition. *Lab Invest*. 2018;98:1159–69.
- Milara J, Peiró T, Serrano A, Cortijo J. Epithelial to mesenchymal transition is increased in patients with COPD and induced by cigarette smoke. *Thorax*. 2013;68:410–20.
- Serrano-Gomez SJ, Maziveyi M, Alahari SK. Regulation of epithelial–mesenchymal transition through epigenetic and post-translational modifications. *Mol Cancer*. 2016;15:18.

13. Su X, Chen J, Lin X, et al. FERMT3 mediates cigarette smoke-induced epithelial-mesenchymal transition through Wnt/ β -catenin signaling. *Respir Res*. 2021;22:286.
14. Mirza S, Clay RD, Koslow MA, Scanlon PD. COPD guidelines: a review of the 2018 GOLD report. *Mayo Clin Proc*. 2018;93:1488–502. <https://doi.org/10.1016/j.mayocp.2018.05.026>.
15. Moll R, Divo M, Langbein L. The human keratins: biology and pathology. *Histochem Cell Biol*. 2008;129:705–33.
16. Jonkman MF, Heeres K, Pas HH, et al. Effects of keratin 14 ablation on the clinical and cellular phenotype in a kindred with recessive epidermolysis bullosa simplex. *J Invest Dermatol*. 1996;107(5):764–9.
17. Liu Y, Lyle S, Yang Z, Cotsarelis G. Keratin 15 promoter targets putative epithelial stem cells in the hair follicle bulge. *J Invest Dermatol*. 2003;121:963–8.
18. Zhan Q, Signoretto S, Whitaker-Menezes D, Friedman TM, Korngold R, Murphy GF. Cytokeratin 15-positive basal epithelial cells targeted in graft-versus-host disease express a constitutive antiapoptotic phenotype. *J Invest Dermatol*. 2007;127:106–15.
19. Kolivras A, Thompson N, Thompson C. Loss of cytokeratin-15 (CK15) expression is not specific for lichen planopilaris (LPP). *J Am Acad Dermatol*. 2016;75:428–9.
20. Giroux V, Stephan J, Chatterji P, et al. Mouse intestinal Krt15+ crypt cells are radio-resistant and tumor initiating. *Stem Cell Reports*. 2018;10:1947–58.
21. Miyashita H, Niwano H, Yoshida S, et al. Long-term homeostasis and wound healing in an in vitro epithelial stem cell niche model. *Sci Rep*. 2017;7:43557.
22. Jih DM, Lyle S, Elenitsas R, Elder DE, Cotsarelis G. Cytokeratin 15 expression in trichoepitheliomas and a subset of basal cell carcinomas suggests they originate from hair follicle stem cells. *J Cutan Pathol*. 1999;26(3):113–8.
23. Sieber-Blum M. Epidermal stem cell dynamics. *Stem Cell Res Ther*. 2011;2(3):29.
24. Tai G, Ranjizad P, Marriage F, et al. Cytokeratin 15 marks basal epithelia in developing ureters and is upregulated in a subset of urothelial cell carcinomas. *PLoS ONE*. 2013;8: e81167.
25. Giroux V, Lento AA, Islam M, et al. Long-lived keratin 15+ esophageal progenitor cells contribute to homeostasis and regeneration. *J Clin Invest*. 2017;127:2378–91.
26. Ilevlev V, Lynch TJ, Freischlag KW, et al. Krt14 and Krt15 differentially regulate regenerative properties and differentiation potential of airway basal cells. *JCI Insight*. 2022;8: e162041.
27. Morris RJ, Liu Y, Marles L, et al. Capturing and profiling adult hair follicle stem cells. *Nat Biotechnol*. 2004;22:411–7.
28. Peng W, Wu Y, Zhang G, et al. GLIPR1 Protects against cigarette smoke-induced airway inflammation via PLAU/EGFR signaling. *Int J Chron Obstruct Pulmon Dis*. 2021;16:2817–32.
29. Wang BQ, Shi M, Zhang JP, et al. Knockdown of TFPI-anchored endothelial cells exacerbates lipopolysaccharide-induced acute lung injury via NF- κ B signaling pathway. *Shock*. 2019;51:235–46.
30. Lu J, Xie L, Liu C, Zhang Q, Sun S. PTEN/PI3K/AKT Regulates macrophage polarization in emphysematous mice. *Scand J Immunol*. 2017;85(6):395–405. <https://doi.org/10.1111/sji.12545>.
31. Agraval H, Yadav UCS. MMP-2 and MMP-9 mediate cigarette smoke extract-induced epithelial-mesenchymal transition in airway epithelial cells via EGFR/Akt/GSK3 β / β -catenin pathway: amelioration by fisetin. *Chem Biol Interact*. 2019;314: 108846.
32. Liu YN, Guan Y, Shen J, et al. Shp2 positively regulates cigarette smoke-induced epithelial mesenchymal transition by mediating MMP-9 production. *Respir Res*. 2020;21:161.
33. Peng L, Wen L, Shi QF, et al. Scutellarin ameliorates pulmonary fibrosis through inhibiting NF- κ B/NLRP3-mediated epithelial-mesenchymal transition and inflammation. *Cell Death Dis*. 2020;11:978.
34. Barnes PJ. Inflammatory mechanisms in patients with chronic obstructive pulmonary disease. *J Allergy Clin Immunol*. 2016;138:16–27.
35. Buttery SC, Zysman M, Vikjord SAA, Hopkinson NS, Jenkins C, Vanfleteren L. Contemporary perspectives in COPD: Patient burden, the role of gender and trajectories of multimorbidity. *Respirology*. 2021;26:419–41.
36. Jiang J, Xu S, Chen Z, Liu W, Zhang L, Li J, Zhu Z, Zhou L. Animal models: an essential tool to dissect the heterogeneity of chronic obstructive pulmonary disease. *J Transl Int Med*. 2023;11(1):4–10.
37. Christenson SA, Smith BM, Bafadhel M, Putcha N. Chronic obstructive pulmonary disease. *Lancet*. 2022;399:2227–42.
38. Singh D. Pharmacological treatment of stable chronic obstructive pulmonary disease. *Respirology*. 2021;26:643–51.
39. Conlon TM, John-Schuster G, Heide D, et al. Inhibition of LT β R signalling activates WNT-induced regeneration in lung. *Nature*. 2020;588:151–6.
40. Waseem A, Dogan B, Tidman N, et al. Keratin 15 expression in stratified epithelia: downregulation in activated keratinocytes. *J Invest Dermatol*. 1999;112:362–9.
41. Bracke KR, Verhamme FM, Seys LJ, et al. Role of CXCL13 in cigarette smoke-induced lymphoid follicle formation and chronic obstructive pulmonary disease. *Am J Respir Crit Care Med*. 2013;188:343–55.
42. Hogg JC, Chu F, Utokaparch S, et al. The nature of small-airway obstruction in chronic obstructive pulmonary disease. *N Engl J Med*. 2004;350:2645–53.
43. Polverino F, Cosio BG, Pons J, et al. B cell-activating factor. An orchestrator of lymphoid follicles in severe chronic obstructive pulmonary disease. *Am J Respir Crit Care Med*. 2015;192:695–705.
44. Faner R, Cruz T, Casserras T, et al. Network analysis of lung transcriptomics reveals a distinct B-cell signature in emphysema. *Am J Respir Crit Care Med*. 2016;193:1242–53.
45. Mizumura K, Cloonan SM, Nakahira K, et al. Mitophagy-dependent necroptosis contributes to the pathogenesis of COPD. *J Clin Invest*. 2014;124:3987–4003.
46. Jacob A, Morley M, Hawkins F, et al. Differentiation of human pluripotent stem cells into functional lung alveolar epithelial cells. *Cell Stem Cell*. 2017;21:472–488.e10.
47. Sun YL, Hurley K, Villacorta-Martin C, et al. Heterogeneity in human induced pluripotent stem cell-derived alveolar epithelial type II cells revealed with ABCA3/SFTPC reporters. *Am J Respir Cell Mol Biol*. 2021;65:442–60.
48. Mercado N, Ito K, Barnes PJ. Accelerated ageing of the lung in COPD: new concepts. *Thorax*. 2015;70:482–9.
49. Aoshiba K, Zhou F, Tsuji T, Nagai A. DNA damage as a molecular link in the pathogenesis of COPD in smokers. *Eur Respir J*. 2012;39(6):1368–76.
50. Vij N, Chandramani-Shivalingappa P, Van Westphal C, Hole R, Bodas M. Cigarette smoke-induced autophagy impairment accelerates lung aging, COPD-emphysema exacerbations and pathogenesis. *Am J Physiol Cell Physiol*. 2018;314:C73–87.
51. Sharafkhaneh A, Hanania NA, Kim V. Pathogenesis of emphysema: from the bench to the bedside. *Proc Am Thorac Soc*. 2008;5:475–7. <https://doi.org/10.1513/pats.200708-126ET>.
52. Tsutsumi A, Ozaki M, Chubachi S, et al. Exposure to cigarette smoke enhances the stemness of alveolar type 2 cells. *Am J Respir Cell Mol Biol*. 2020;63:293–305.
53. Vlahos R, Wark PA, Anderson GP, Bozinovski S. Glucocorticosteroids differentially regulate MMP-9 and neutrophil elastase in COPD. *PLoS ONE*. 2012;7: e33277.
54. Zhou L, Le Y, Tian J, et al. Cigarette smoke-induced RANKL expression enhances MMP-9 production by alveolar macrophages. *Int J Chron Obstruct Pulmon Dis*. 2019;14:81–91.
55. Zhao Y, Qiao X, Wang L, et al. Matrix metalloproteinase 9 induces endothelial-mesenchymal transition via Notch activation in human kidney glomerular endothelial cells. *BMC Cell Biol*. 2016;17:21.

Publisher's Note

Springer Nature remains neutral with regard to jurisdictional claims in published maps and institutional affiliations.